

**MARS 2001 ODYSSEY  
NEUTRON COMPONENT OF THE  
MARS ODYSSEY GRS SUITE OF INSTRUMENTS  
Version 1.0**

11/01/2002

Prepared by:  
W.C. Feldman

**Table of Contents**

1. Introduction.....	3
2. Sensor Configuration .....	3
3. Neutron Component Identification .....	3
4. Sensor Electronics.....	4
5. Event-Mode Data.....	5
6. Experimental Signature of a Fast Neutron Event .....	5
6.1. Laboratory Calibration.....	5
6.2. Fast-Neutron Identification Aboard Mars Odyssey .....	6
6.3. Simulated Fast Neutron Response Function.....	7
7. Determination of the Spectrum of Fast Neutrons .....	8
7.1. AmB Calibration.....	8
7.2. Thermal and Epithermal Neutron Calibrations.....	9
8. References.....	9

## 1. INTRODUCTION

This shortened writeup of the NS component of the GRS suite of instruments aboard Mars Odyssey is excerpted from a more complete writeup that was published in JGR [Feldman et al., 2002].

## 2. SENSOR CONFIGURATION

The Mars Odyssey neutron sensor consists of a cubical block of boron-loaded plastic scintillator (marketed by Bicon Corporation as BC454) having dimensions of 11 x 11 x 10 cm. It is segmented into four prism-shaped quadrants as shown in Figure 1. The prism segments are optically isolated from one another, and each is viewed by a separate 3.8-cm diameter photomultiplier tube (PMT). A white reflector completely surrounds each of the four prisms to ensure maximum light coupling to the PMTs while maintaining optical isolation.

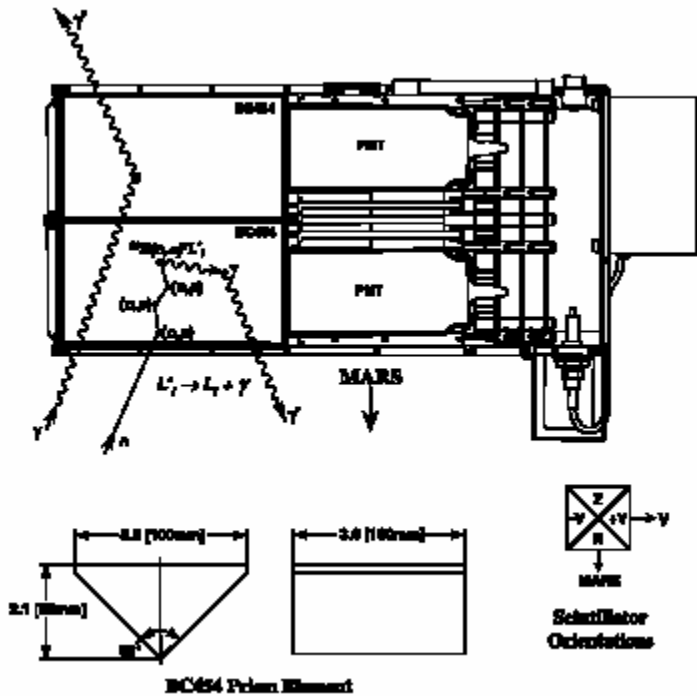


Figure 1. (top) A cut through the Mars Odyssey neutron spectrometer and (bottom) details of one of the four BC454 prism elements. Superimposed on the drawing at top is a schematic illustration of possible interactions between gamma rays and neutrons with the sensor elements of the neutron spectrometer. Also shown beneath the line drawing is the orientation of the detector in orbit about Mars.

## 3. NEUTRON COMPONENT IDENTIFICATION

Borated plastic scintillator has a heritage of space applications for detecting neutrons and uniquely identifying them as such in the presence of backgrounds of gamma rays and energetic charged particles that are generally encountered in space [Feldman et al., 1991, 1999]. Thermal and epithermal neutrons are identified by detection of a single interaction that deposits an energy equal to the Q value of the  $^{10}\text{B}(n,\alpha)^7\text{Li}^*$  reaction in one or two of the sensor prism segments. This Q value energy (2.8 MeV) is split between the recoil energies of the alpha particle and  $^7\text{Li}$  nucleus produced in the reaction, and a gamma ray from the transition between the first excited state of  $^7\text{Li}$  (populated 94% of the time) and its ground state. Because of a pulse-height defect in plastic scintillator, the energy deposition of both nuclear recoils in the  $^{10}\text{B}(n,\alpha)^7\text{Li}^*$  reaction appears as a 93 keV electron, which is termed throughout this writeup as an equivalent electron energy,  $E_{eq}$ . The signature of a fast neutron is the detection of a pair of interactions occurring within  $5\ \mu\text{s}$  (the pulse-correlation time for fast neutrons interacting in BC454 is about  $t=2\ \mu\text{s}$ ). The first interaction of the pair corresponds to the transfer of incident neutron energy to proton recoils in the plastic and the second interaction corresponds to the  $^{10}\text{B}(n,\alpha)^7\text{Li}^*$  reaction. This sequence is pictured schematically in the top part of Figure 1. The second interaction occurs in isolation if the incident neutron has energy less than about 0.7 MeV, which is then the signature of a thermal or epithermal neutron. If a pair of interactions is detected, then the pulse height of the first interaction provides a measure of the energy of the fast neutron.

Separate determinations of the thermal, epithermal, and fast flux components of Martian and spacecraft neutron flux spectra is optimized by orienting the sensor block such that one of its prism segments faces in the direction of the spacecraft velocity vector (forward), one faces in the opposite direction (backward), one faces downward toward the Martian surface (nadir), and one faces upward (zenith), toward the spacecraft. This configuration has the advantage that it allows discrimination between neutrons that originate in Mars and those originating in the spacecraft, without the need of a boom.

Given this orientation (as pictured in Figure 1), all three energy components of the neutron flux from both the spacecraft and Mars can be measured and separately identified (see e.g., Feldman and Drake [1986] for the thermal and epithermal neutron components). Specifically, the difference in counting rates of the forward- and backward-facing BC454 prism segments provides a measure of thermal neutrons from Mars alone. Contamination by thermals from the spacecraft and all epithermal neutrons are removed by virtue of the motion of the sensor relative to Mars, as opposed to its co-motion relative to the spacecraft. The motion of the sensor relative to Mars ( $3.4 \text{ km s}^{-1}$  in the mapping orbit at an altitude of 400 km) ensures that the forward-facing prism segment selectively scoops up the thermals from Mars, but the backward-facing prism segment outruns them. For an average surface temperature at Mars of 220 K, the speed of a thermal neutron is  $1.9 \text{ km s}^{-1}$ . The fact that all four prism segments are stationary relative to the spacecraft ensures that the fraction of spacecraft contributions to each prism segment is fixed by geometry, which can be measured during cruise and non-mapping orientations while in orbit about Mars.

The nadir pointing face of the NS, which is not subject to a Doppler change in counting rate, is covered by 0.69 mm thick sheets of Cd on all outwardly exposed surfaces. It is therefore only sensitive to neutrons having energies greater than 0.4 eV, which lies within the epithermal energy range. It is shielded from the spacecraft by the other three prisms and so provides a measure of epithermal neutrons from Mars alone.

All four prism segments can be used to provide separate measures of Martian and spacecraft fast neutrons. As for the epithermals, but to a lesser extent, this separation is facilitated by the absorption properties of the geometric arrangement of all four BC454 prism segments relative to the surface of Mars and the spacecraft. This approach is only feasible for this kind of an arrangement because the hydrogen moderator in the sensor is contained in an active element of the detector (the BC454 scintillators). This situation is significantly different from containment in a passive element such as is provided by a polyethylene (or equivalent) moderator that is placed around a thermal neutron sensor.

#### **4. SENSOR ELECTRONICS**

For fast neutron detection and identification, the front-end electronics (FEE) of the NS is designed to recognize compound events consisting of two interactions within  $25.6 \mu\text{s}$  and to measure the elapsed time (time-to-second pulse (TTSP)) between them. Both first- and second-interaction pulse heights are separately digitized using 8-bit analog-to-digital converters (ADCs).

Two categories of events are recognized by the FEE. These categories correspond to the following: (1) A category 1 event is a first (prompt) BC454 interaction having energy in the range  $40 \text{ keVeq} < E1 < 630 \text{ keVeq}$  that is not followed by a second (delayed) interaction within  $25.6 \mu\text{s}$ . Another characteristic is that the interaction should be registered in only one or two prism segments of the neutron sensor. Any prompt interaction having energy greater than 2.55 MeVeq (regardless of the number of sensor elements that register energy above threshold) will be identified as a galactic cosmic ray (GCR). After detection, no second interaction is looked for, and the event is counted in a dedicated GCR scaler. (2) A category 2 event is a prompt BC454 interaction having energy in the range  $40 \text{ keVeq} < E1 < 2.55 \text{ MeVeq}$  that deposits energy in one or two

prism segments only and that is followed by a second (delayed) interaction that is detected in one or two prism segments within a  $25.6\text{-}\mu\text{s}$  gate window beginning with the time of the first interaction. The second interaction must have energy in the range  $40 \text{ keVeq} < E2 < 630 \text{ keVeq}$ . Any event that does not satisfy these criteria is ignored but is nevertheless accounted for in a dedicated dead-time counter.

From the previous definitions, we see that the electronic separation of detected events into category 1 and category 2 defines an experimental discrimination between the thermal-epithermal and fast neutron energy ranges, respectively.

## 5. EVENT-MODE DATA

For every category 2 event identified by onboard classification firmware, information used in the present study to determine the energy spectrum of fast neutrons aboard Mars Odyssey consist of (1) a 5-bit prompt ADC address, (2) a 6-bit delayed ADC address, (3) a 4-bit prompt interaction sensor ID, (4) a 1-bit delayed interaction sensor ID, and (5) an 8-bit digitized TTSP. The prompt and delayed ADC addresses give the pulse height of the prompt and delayed interactions, respectively. Each of the four prompt interaction ID bits identifies a unique prism that detects energy deposition above threshold. Only one or two prisms are allowed for analysis. The delayed ID bit identifies only whether the second interaction occurred in one or two prisms. Here again, three- and four-prism events are rejected by the onboard event classifier.

Event-mode data consist of the first 84 3-byte events in each accumulation time interval. All succeeding events are counted without recording details of the separate interactions.

## 6. EXPERIMENTAL SIGNATURE OF A FAST NEUTRON EVENT

### 6.1. Laboratory Calibration

The Mars Odyssey NS was calibrated for fast neutrons using both an AmB and a  $^{252}\text{Cf}$  source. We will only report an analysis of the AmB data here. The measured neutron energy spectrum of an AmB source normalized to unit fluence is shown in Figure 2 [Marsh et al., 1995]. It is seen to have a single broad peak at 2.9 MeV.

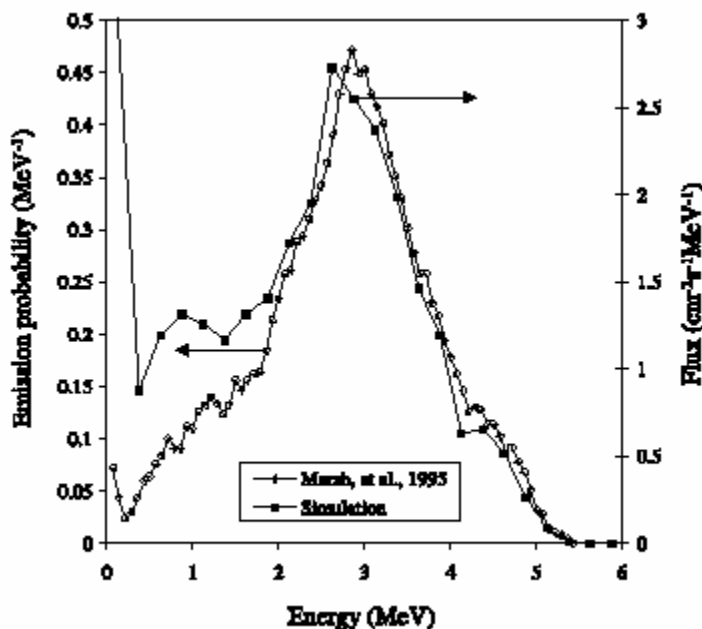


Figure 2. The fast neutron spectrum directly emitted by an AmB neutron source (given by open circles) [Marsh et al., 1995] and as modified by the Pb shielding used in the NS laboratory calibration as well as by the concrete floor of the laboratory.

The strength of our AmB source is  $2 \times 10^5 \text{ s}^{-1}$ . It was placed within a hollow cylindrical Pb shield having 10 cm OD, 4 cm ID, and 4.5-cm length to eliminate the 59.7 keV gamma rays from the  $^{241}\text{Am}$  alpha emitter of the source. This shield was resting on a 10 x 5 x 20 cm Pb brick, which, in turn, was supported by an empty cardboard box so that the source was, for all practical purposes, floating 106 cm above the thick concrete floor of our laboratory. The neutron spectrometer was supported by another empty cardboard box 93 cm above the floor and 50 cm from the source. Both source and detector were placed in the middle of the laboratory, each 1.5 m from the nearest wall, which was made of plasterboard construction.

The gains of all PMTs were matched and calibrated using a variety of sources, given in Table 2. Effective energies of the Compton edges of the sources were determined using the prescription developed by Cherubini et al. [1989]. A

straight line fits the data quite well, which yields a channel at zero energy of  $C0 = -1.1$ , which we assume to be independent of PMT gain and time.

## 6.2. Fast-Neutron Identification Aboard Mars Odyssey

The NS component of the Mars Odyssey GRS was operated for about 5 months during cruise. For this study we concentrate on 45,000 19.2-s spectral accumulation periods measured during the relatively quiet conditions that prevailed between 1 and 10 July 2001. The histogram of TTSP for this time period is shown in Figure 3 and that of the single (top line) and double (bottom line) prism second-interaction pulse height distributions are shown in Figure 4. The histogram of TTSP, together with the pulse-height spectrum of the second interaction of each category 2 event, provides a unique signature of a fast neutron that has lost all of its measurable energy in the detector. Starting first with the histogram of TTSP, the upper data points give the data as measured. Inspection shows a constant rate for times larger than 15  $\mu\text{s}$  and clearly enhanced counting rates at times less than 7  $\mu\text{s}$ . The rate at late times represents chance coincidences, given by the probability that no interaction occurs in the time  $T$  between the first and second interactions,  $\exp(-RT)$ , times the probability of detecting an interaction in time interval  $\Delta T = 0.1 \mu\text{s}$ , which is given by  $R\Delta T$  provided that  $R\Delta T \ll 1$ . Here  $R$  is the total counting rate of the detector. For the low rates encountered between 1 and 10 July 2001 (the measured counting rate was less than  $600\text{s}^{-1}$ ),  $RT$  is small and the late-time counting rate is then independent of time, as given by the horizontal line in Figure 3.

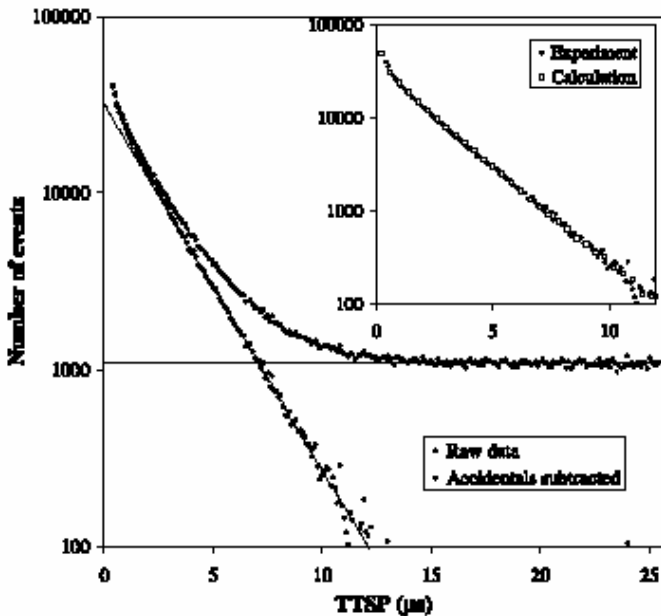


Figure 3. Histograms of the time to second pulse before and after subtraction of chance-coincidence counting rates measured between July 1 and 10, 2001 aboard Mars Odyssey. An overlay of our simulated with the measured time-to-second pulse (TTSP) is shown at the top right. See the text for details.

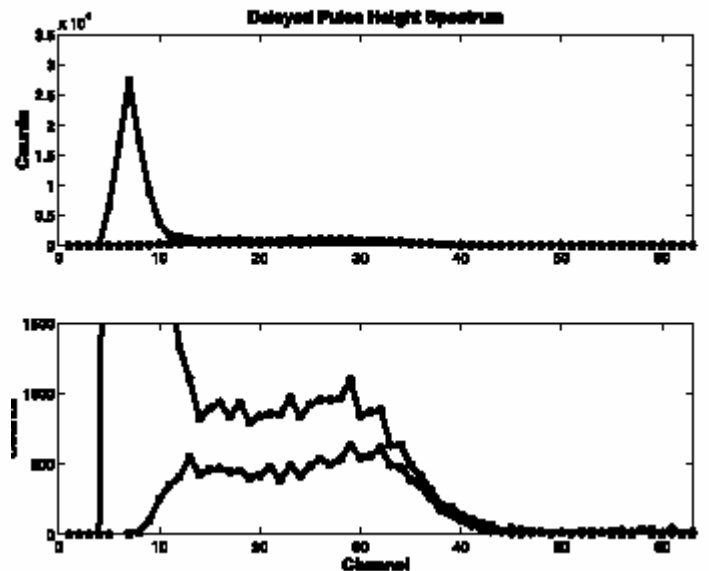


Figure 4. Histograms of delayed interactions that deposit all of their sensible energy in only one prism (the top line in both panels) or two prisms (the bottom line in both panels) measured between 1 and 10 July 2001 aboard Mars Odyssey. See the text for details.

After subtraction of the constant chance coincidence rate from the measured rate, we get the lower data set in Figure 3. This result can be fit by an exponential for times between 3 and 10  $\mu\text{s}$ , yielding a time constant,  $t = 2.09 \mu\text{s}$ , as shown in Figure 3. This time is close to expectations for a 5% loading of natural boron in a very large volume plastic scintillator [Kamykowski, 1990; Feldman et al., 1991; Byrd and Urban, 1994]. Although we note an excellent fit by a single exponential over 2 orders of magnitude, the data are systematically high relative to the fit at the very earliest times. This effect shows up as well in the simulations and has been attributed to the finite size of the sensor

[Kamykowski, 1990; Byrd and Urban, 1994]. An overlay of our simulations of TTSP for the Mars Odyssey NS (which will be described shortly) and the measured TTSP during cruise is shown in the inset panel to the top right in Figure 3. The fit is seen to be excellent.

In order to extract the spectral signature of the  $^{10}\text{B}(n,\alpha)^7\text{Li}^*$  reaction from the second-interaction histograms, chance coincidence events must be subtracted from the real plus chance coincidence events at early times. This task is accomplished by splitting all the event-mode data into early and late time groups. For this purpose, early times are defined as all TTSP between 0.4 and 5.4  $\mu\text{s}$ , and late times are those for which TTSP is between 20 and 25  $\mu\text{s}$ . Histograms of early minus late time counts for the single- and double-prism second interactions are shown in Figure 4.

**Table 1.** Energy Calibration Sources for the Mars Odyssey NS. Effective Compton edge energies are given by Cherubini et al. [1989] corresponding to the channel at half the height of the Compton peak.

Source	Type of Radiation	Effective Energy, keV
241Am	full energy gamma-ray peak	59.7
$^{10}\text{B}(n,\alpha)^7\text{Li}$	charged-particle recoil	93
$^{133}\text{Ba}$	Compton edge, gamma ray	227
$^{22}\text{Na}$	Compton edge, gamma ray	372
$^{137}\text{Cs}$	Compton edge, gamma ray	503

Inspection of the single-prism histogram shows a large peak at about channel 7 followed by a broad plateau extending out to about channel 35. This shape is the unique signature of the  $^{10}\text{B}(n,\alpha)^7\text{Li}^*$  reaction. Here, the low-energy peak corresponds to the charged-particle recoils in the plastic, which appears at an equivalent electron energy  $E_{\text{eq}}$  of 93 keV [Feldman et al., 1991]. The broad plateau corresponds to the coincident detection of the charged-particle recoil with the Compton interaction of the gamma ray de-excitation of the first excited state of  $^7\text{Li}$ . The foregoing interpretation of this plateau as a Compton interaction is verified by the spectrum of two-prism second interactions, shown by the lower curve in Figure 4. Here, the Compton edge is seen to be at about channel 35, and the counting rate at low energies is cut off at about channel 10. This cutoff is expected because the 478-keV gamma transition is in coincidence with the  $^7\text{Li}$  particle recoils of the  $^{10}\text{B}(n,\alpha)^7\text{Li}^*$  reaction. As seen by the single-prism spectrum, this energy deposition shifts the Compton spectrum to the right by about 10 channels, which at the time of these measurements correspond to 93 keV<sub>eq</sub>.

We note that above the Compton edge of this interaction the counts drop to zero. This observation demonstrates the low background that is inherent in an identification of a fast neutron by BC454. Delayed interactions having pulse heights less than channel 5 are present in the spectrum as measured but were eliminated from our analysis. These events correspond to after pulsing in the PMTs and have a relatively low intensity. We conclude that detection and identification of fast neutrons by the NS aboard Mars Odyssey is very clean.

### 6.3. Simulated Fast Neutron Response Function

Before proceeding to an analysis of the measured pulse-height spectra of prompt-interaction events for our AmB calibration and Mars Odyssey flight data, we need to determine the energy dependence of the effective area of the NS sensor. A general geometry Monte Carlo neutron transport code was written, which tracks the light output from separate prompt and delayed interactions as well as the time difference between them (T. H. Prettyman et al., manuscript in preparation, 2002). The code models coincidence signatures for neutron spectrometers used for planetary science. The Mars NS sensor model included an exact treatment of the segmented geometry of the scintillation detectors and surrounding neutron-absorbing and neutron-scattering materials. Events were accepted for analysis only if light output was detected above an equivalent electron energy  $E_{\text{eq}}=40$  keV in one and only one prism. A uniform distribution of neutron energies between 0.25 and 10 MeV, sorted into 0.25-MeV bins, was used for this purpose. For the interpretation of laboratory data the simulation consisted of a parallel beam of neutrons incident on one of the prisms. For interpreting cruise data and data acquired at Mars a second simulation was carried out with neutrons having incidence directions uniformly distributed within the solid angle that will be subtended by Mars when Mars Odyssey is in its mapping orbit at an altitude of 400 km. An overview of the full set of response functions is given at the top of Figure 5. Here, the X axis of the simulated response matrix corresponds to the energy of the neutron incident on the sensor,  $E$ , the Y axis corresponds to the light output of prompt interactions, given in equivalent electron energy,  $E_{\text{eq}}$ , and the Z axis is coded according to the color bar at the right, given in  $\log_{10}$  of effective area in  $\text{cm}^2$ .

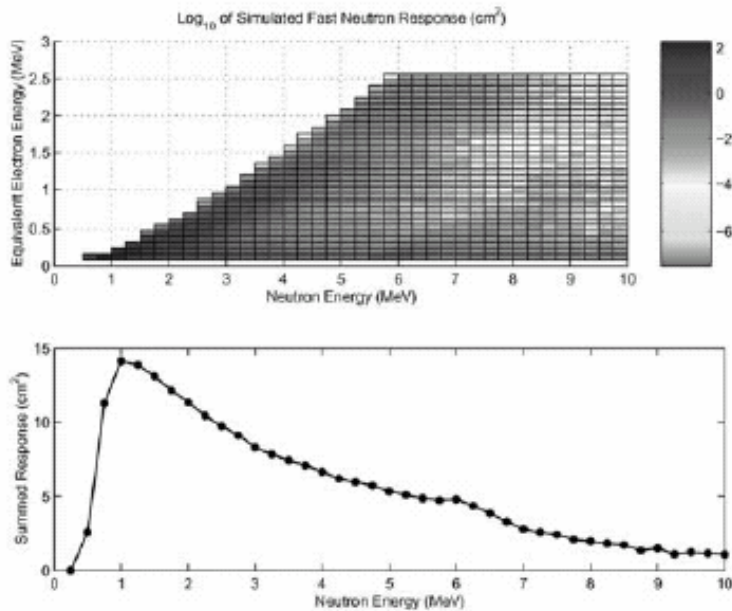


Figure 5. (top) Simulated fast neutron response functions (or effective area in cm<sup>2</sup>) for an isotropic distribution of neutrons incident normal to one of the prisms of the sensor having prescribed energies. (bottom) The response matrix summed over all equivalent electron energies (which is along the y axis in the top panel) is given in units of cm<sup>2</sup>. See the text for details.

A sum over all equivalent electron energies giving the total area- efficiency product as a function of incident neutron energy, is shown at the bottom of Figure 5. The cutoff at low energy reflects the discriminator threshold for detection of a prompt interaction, and the roll-over above 6 MeV reflects the upper range of the analog electronics, set at  $E_{eq} = 2.55$  MeV .

## 7. DETERMINATION OF THE SPECTRUM OF FAST NEUTRONS

### 7.1. AmB Calibration

We can test our procedure by analyzing the AmB calibration data. The first step in this analysis is to generate the actual spectrum of neutrons incident on the detector after the source spectrum is modified by passage through the Pb shield and reprocessed by the concrete floor of the laboratory. This spectrum was simulated using MCNP4C and is compared with the emitted spectrum in Figure 2.

The next step in our analysis was to fold the simulated AmB spectrum at the sensor with the calculated response functions in Figure 5. An overlay of the simulated and measured spectra is shown in Figure 6. Here, the measured spectrum is determined from the measured counting rates by correcting for the detector dead time and the ratio of total two-interaction events recorded per spectrum to the 84 events per spectrum allowed by the size of our telemetry buffer. Whereas the first correction amounted to a factor of 1.029, the second was 65.1. Inspection of Figure 6 shows that the correspondence between simulated and measured spectra is excellent. Summation over energy of the counts in the measured and simulated spectra yields 32.8 and 31.1, respectively. They differ by 5.5%. This agreement validates our technique for determining absolute fast-neutron spectra from measured NS counting-rate spectra. We therefore expect our uncertainties to be no more than 5%.

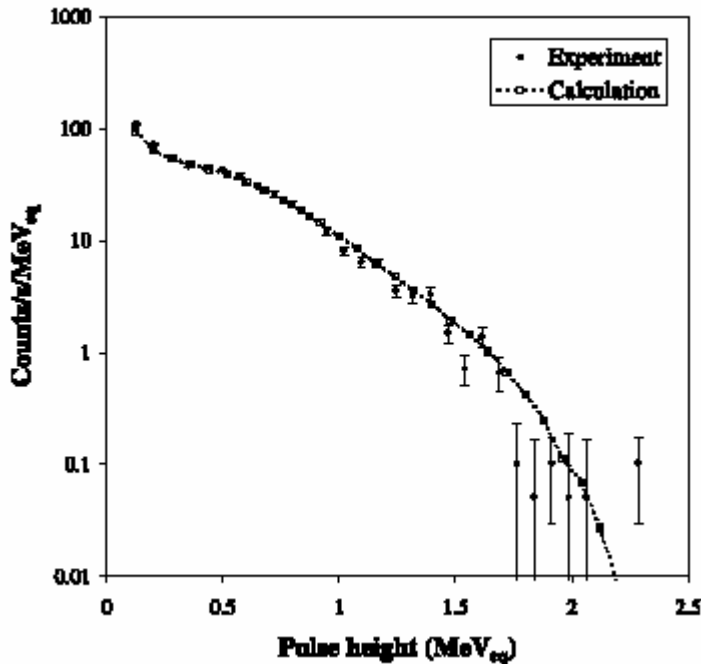


Figure 6. Energy spectrum of fast neutrons measured during the AmB calibration in the laboratory before launch (solid squares) and folded with the simulated sensor response function (open circles) using the known spectrum of AmB [Marsh et al., 1995] as modified by the laboratory set up.

## 7.2. Thermal and Epithermal Neutron Calibrations

The response of NS to thermal neutrons was measured using a  $1 \times 10^7 \text{ s}^{-1}$  AmBe neutron source placed in the center of a  $152 \times 152 \times 244$  cm reactor-grade graphite pile at Los Alamos. Spectra for each of the prism segments as a function of the angle between their front surface normals and the normal to the pile were measured. These spectra were similar to that shown in Figure 3. Because of the press of work to fully validate the first results from Mars orbit; these spectra have not been intercompared with simulations of the sensor response to thermal neutrons.

The response of the NS to epithermal neutrons was measured using the  $2 \times 10^5 \text{ s}^{-1}$  AmB source used for the fast neutron calibration mentioned previously. This source was placed into the center of a  $35 \times 35 \times 46$  cm block of reactor-grade graphite. This block was completely surrounded by a 2.5 cm thick veneer of polyethylene. Spectra for each of the prism segments as a function of the angle between their front surface normals and the normal to one of the faces of this graphite block were measured. These spectra were also similar to that shown in Figure 3. Because of the press of work to fully validate the first results from Mars orbit, these spectra have not been intercompared with simulations of the sensor response to the combined output of thermal and epithermal neutrons that emanate from this block.

## 8. REFERENCES

Byrd, R. C., and W. T. Urban, Calculations of the neutron response of boron-loaded scintillators, Los Alamos Rep. LA-12833-MS, Los Alamos Natl. Lab., Los Alamos, N.M., 1994.

Cherubini, R., G. Moschini, R. Nino, R. Policroniades, and A. Varela, Bamma calibration of organic scintillators, Nucl. Instrum. Methods Phys. Res., Sect. A, 281, 349–352, 1989.

Feldman, W. C., and D. M. Drake, A Doppler filter technique to measure the hydrogen content of planetary surfaces, Nucl. Instrum. Methods Phys. Res., Sect. A, 245, 182–190, 1986.

Feldman, W. C., G. F. Auchampaugh, and R. C. Byrd, A novel fast-neutron detector for space applications, Nucl. Instrum. Methods Phys. Res., Sect. A, 306, 350–365, 1991.

Feldman, W. C., B. L. Barraclough, K. R. Fuller, D. J. Lawrence, S. Maurice, M. C. Miller, T. H. Prettyman, and A. B. Binder, The Lunar Prospector gamma-ray and neutron spectrometers, Nucl. Instrum. Methods Phys. Res., Sect. A, 422, 562–566, 1999.

Feldman, W.C., T.H. Prettyman, R.L. Tokar, W.V. Boynton, R.C. Byrd, K.R. Fuller, O. Gasnault, J.L. Longmire, R.H. Olsher, S.A. Storms, and G.W. Thornton, Fast neutron flux aboard Mars Odyssey during cruise, J. Geophys. Res., 107:A6, 10,1029-10,1040, 2002.

Kamykowski, E. A., Analysis of mean lifetime for capture of neutrons in boron loaded plastic scintillators, Nucl. Instrum. Methods Phys. Res., Sect. A, 299, 105–110, 1990.

Marsh, J. W., D. J. Thomas, and M. Burke, High resolution measurements of neutron energy spectra from Am-Be and Am-B neutron sources, Nucl. Instrum. Methods Phys. Res., Sect. A, 366, 340–348, 1995.